

Analogy between periodic patterns in thin smectic liquid crystal films and the intermediate state of superconductors

Bruno Zappone, Atilla Eren Mamuk, Iryna Gryn, Valentina Arima, Alessandra Zizzari, Roberto Bartolino, Emmanuelle Lacaze, Rolfe Petschek

▶ **To cite this version:**

Bruno Zappone, Atilla Eren Mamuk, Iryna Gryn, Valentina Arima, Alessandra Zizzari, et al.. Analogy between periodic patterns in thin smectic liquid crystal films and the intermediate state of superconductors. Proceedings of the National Academy of Sciences of the United States of America, 2020, 117 (30), pp.17643-17649. 10.1073/pnas.2000849117 . hal-03070716

HAL Id: hal-03070716
https://hal.science/hal-03070716

Submitted on 15 Dec 2020

HAL is a multi-disciplinary open access archive for the deposit and dissemination of scientific research documents, whether they are published or not. The documents may come from teaching and research institutions in France or abroad, or from public or private research centers.

L'archive ouverte pluridisciplinaire **HAL**, est destinée au dépôt et à la diffusion de documents scientifiques de niveau recherche, publiés ou non, émanant des établissements d'enseignement et de recherche français ou étrangers, des laboratoires publics ou privés.

Please use this PDF proof to check the layout of your article. If you would like any changes to be made to the layout, you can leave instructions in the online proofing interface. Making your changes directly in the online proofing interface is the quickest, easiest way to correct and submit your proof. Please note that changes made to the article in the online proofing interface will be added to the article before publication, but are not reflected in this PDF proof.

Q:1, 2, 3, 4, 5

Analogy between periodic patterns in thin smectic liquid crystal films and the intermediate state of superconductors

Bruno Zappone[a,1], Atilla Eren Mamuk[b], Iryna Gryn[c], Valentina Arima[d], Alessandra Zizzari[d], Roberto Bartolino[c], Emmanuelle Lacaze[e], and Rolfe Petschek[f]

[a]Consiglio Nazionale delle Ricerche, Istituto di Nanotecnologia, c/o Dipartimento di Fisica, Università della Calabria, 87036 Rende (CS), Italy; [b]Laboratory of Liquid and Solid Crystals, Department of Physics, Muğla Sitki Koçman University, TR48000, Muğla, Turkey; [c]Dipartimento di Fisica, Università della Calabria, 87036 Rende (CS), Italy; [d]Consiglio Nazionale delle Ricerche, Istituto di Nanotecnologia, c/o Campus Ecotekne, Università del Salento, 73100 Lecce, Italy; [e]Institut des Nano-Sciences de Paris, CNRS, Sorbonne Université, 75005 Paris, France; and [f]Department of Physics, Case Western Reserve University, Cleveland, OH 44106

Edited by Robert J. Birgeneau, University of California, Berkeley, CA, and approved June 4, 2020 (received for review January 30, 2020)

Spontaneous breaking of symmetry in liquid crystal (LC) films often reveals itself as a microscopic pattern of molecular alignment. In a smectic-*A* LC, the emergence of positional order at the transition from the nematic phase leads to periodic textures that can be used as optical microarrays, templates for soft lithography, and ordering matrices for the organization and manipulation of functional nanoparticles. While both 1d and 2d patterns have been obtained as a function of the LC film thickness and applied fields, the connection has not been made between pattern formation and the peculiar critical behavior of LCs at the nematic–smectic transition, still eluding a comprehensive theoretical explanation. In this article, we demonstrate that an intense bend distortion applied to the LC molecular director while cooling from the nematic phase produces a frustrated smectic phase with depressed transition temperature, and the characteristic 1d periodic texture previously observed in thin films and under applied electric fields. In light of De Gennes' analogy with the normal-superconductor transition of a metal, we identify the 1d texture as the equivalent of the intermediate state in type I superconductors. The bend distortion is analog to the magnetic field in metals and penetrates in the frustrated phase as an array of undercooled nematic domains, periodically intermixed with bend-free smectic-*A* domains. Our findings provide fundamental evidence for theories of the nematic–smectic transition, highlighting the deep connection between phase frustration and pattern formation, and perspectives on the design of functional smectic microarrays.

liquid crystals | superconductors | phase transitions | pattern formation | phase frustration

Liquid crystals (LCs) commonly used in displays and optical devices are composed of rod-like molecules that tend to align along a common director **n** depending on external aligning fields such as surface interactions (anchoring) and electric fields (1). The molecular density is uniform in the nematic (*N*) phase, whereas a 1d density modulation (i.e., layering) appears in the smectic phase. There are several kinds of smectic phases with different types of molecular order and alignment, and the one showing a density modulation along the director **n** is called smectic-*A* (*S*) phase (1). It has long been known that conflicting aligning fields can induce defect nucleation, and formation of 1d and 2d micropatterns in the *S* phase (2–10). More recently, pattern formation has been recognized as a promising platform for the rapid and cost-effective bottom-up fabrication of optical microarrays (11–13), templates for soft lithography (14–17), and anisotropic matrices for ordering and guiding the assembly of functional nanoparticles (9, 18–21). LCs also provide the advantage of a fast and large response to external stimuli, e.g., smectic patterns can change morphology as a function of an applied electric or magnetic field (10, 22, 23).

Very few studies have addressed the connection between pattern formation and the peculiar critical behavior of LCs at the *N*–*S* transition (23–25), which stands out as a major theoretical challenge in statistical mechanics and condensed matter physics (26). Insights can be gained from an analogy between smectics and superconductors, first pointed out by De Gennes (27). In both materials, the Landau–Ginzburg free energy expansion involves a complex parameter $\psi = |\psi|e^{i\varphi}$ and a vector field **n**. In metals, $|\psi|$ is the density of Cooper electron pairs and $\mathbf{B} = \nabla\times\mathbf{n}$ is the magnetic field. At the transition to the low-temperature superconducting state, **B** tends to be expelled from the bulk (Meissner effect, Fig. 1). A field with amplitude B is expelled below a critical temperature $T_c(B)$ that increases as B is decreased, i.e., $T_c(B) \leq T_0$ with $T_0 = T_c(0)$. At a temperature $T < T_0$, the field is expelled below a critical amplitude $B_c(T)$ that increases as T is decreased. At temperatures and fields immediately below the critical values, the expulsion is incomplete and inhomogeneous, and **B** penetrates in the superconductor, i.e., the superconductor phase is frustrated. In a type I superconductor film, finite-sized domains of undercooled normal metal state, carrying the **B** field, become intermixed with superconductive domains in a pattern of meandering stripes or polygonal meshes known as intermediate state (28–30) (Fig. 1).

Significance

Microscopic patterns of molecular alignment are easily obtained in smectic LCs subject to conflicting alignment conditions and provide a promising route to the rapid bottom-up fabrication of ordered materials, notably for the organization and manipulation of nanoparticles. A convenient but puzzling feature is that the pattern type can be switched between 1d and 2d by varying the film thickness or applying an electric field. We devised a simple experiment to show that 1d patterns are due to frustration of the smectic phase under a strong distortion of the molecular director field, leading to a mixed nematic–smectic phase. Our finding confirms the long-standing prediction of an "intermediate" LC state based on an analogy with superconductors.

Author contributions: B.Z. designed research; B.Z., A.E.M., I.G., V.A., A.Z., R.B., E.L., and R.P. performed research; B.Z., A.E.M., and I.G. analyzed data; and B.Z. wrote the paper.

The authors declare no competing interest.

This article is a PNAS Direct Submission.

Published under the PNAS license.

[1]To whom correspondence may be addressed. Email: bruno.zappone@cnr.it.

This article contains supporting information online at https://www.pnas.org/lookup/suppl/doi:10.1073/pnas.2000849117/-/DCSupplemental.

PROOF FINAL EMBARGOED

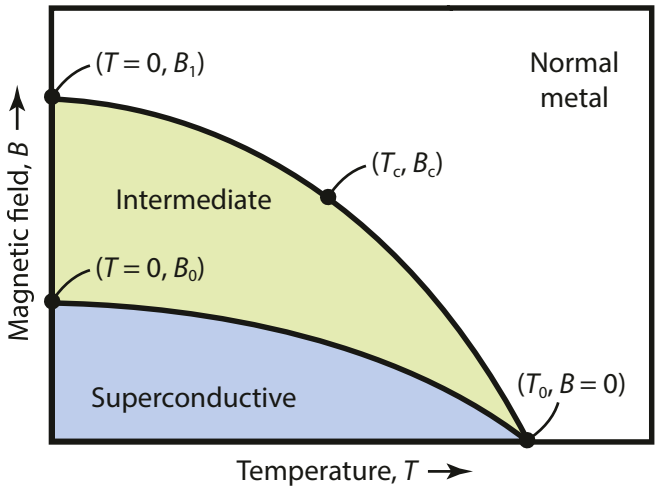


Fig. 1. Schematic phase diagram of a type I superconductor showing a frustrated intermediate state between the normal metal and superconductive states. The magnetic field B is completely expelled from the latter state, whereas it penetrates in the intermediate state via finite-sized domains of undercooled normal metal. T_c and B_c are the critical temperature and field of the transition from the normal state.

In type II superconductors, **B** penetrates via a 2d array of elementary defects (vortices) known as Abrikosov lattice (28).

In LCs, $|\psi|$ is the amplitude of the 1d smectic density modulation and the rotor field $\nabla\times\mathbf{n}$ is associated with twist and bend director distortions (1, 27). The phase φ is constant on surfaces (known as smectic "layers") that are normal to the wave-vector $\mathbf{q} = \nabla\varphi$ of the density modulation. In an undistorted smectic LC, the spacing $2\pi/q$ between layers is constant ($q = q_0$) and $\mathbf{q} \,||\, \mathbf{n}$. In analogy with superconductors, $\nabla\times\mathbf{n}$ tends to be expelled at the transition from the N phase to the low-temperature S phase, which is equivalent to imposing constant spacing or confocality of (curved) smectic layers (27). De Gennes' analogy famously led to the discovery of twist grain boundary phases in chiral thermotropic LCs, where the twist field penetrates as a set of periodically spaced screw dislocations analog to the Abrikosov vortex lattice (31, 32). On the other hand, very few studies have focused on type I behavior (33–35), even though the molecular structure of common thermotropic LCs used in displays and optics produces this behavior (1, 31). In particular, the "intermediate" LC state predicted by De Gennes has never been clearly identified (27).

Results

The common thermotropic LC compound 4-cyano-4′-octylalkylbiphenyl (8CB), showing a bulk N–S transition at 32.5 °C, was confined between two parallel glass surfaces. One surface was coated with a thin layer of polymer and gently rubbed along the x direction to align the LC molecules along x, i.e., induce unidirectional (nondegenerate) planar anchoring at the surface. The other surface was coated with a monolayer of surfactant to align the molecules along the surface normal z, i.e., induce homeotropic (normal) anchoring. Such boundary conditions are known as unidirectional (nondegenerate) hybrid anchoring conditions. In the N phase, they induce a splay-bend distortion of the director field **n** in the xz plane, i.e., with components n_x and n_z depending on z, and perpendicular component $n_y = 0$. Pattern formation was studied as a function of the LC film thickness h and temperature T in regions showing a sharp step-like variation of h, obtained by etching the glass surfaces with a corrosive acid solution.

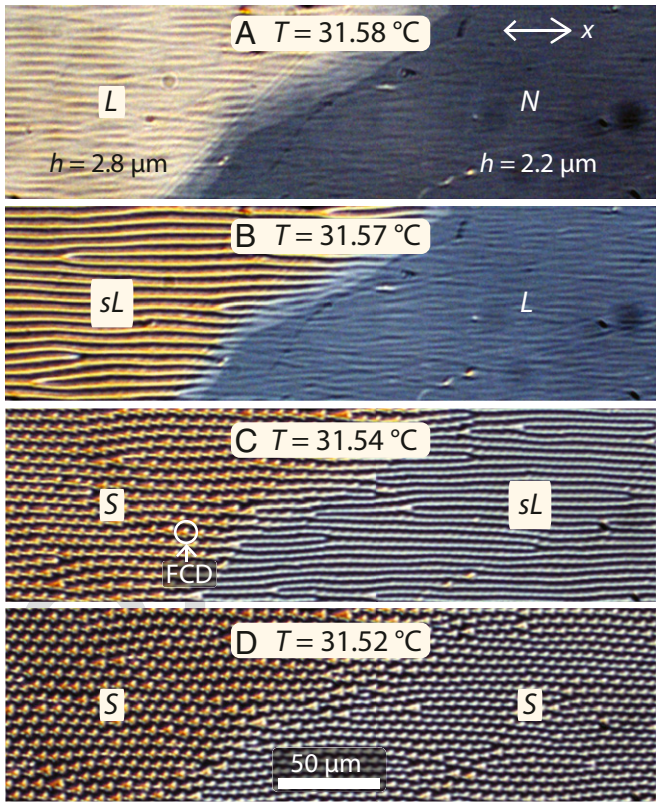


Fig. 2. Textures observed across a step of thickness upon cooling an 8CB Q:13 film with large thickness, $h \geq 2.0$ μm, under unidirectional hybrid anchoring conditions. The step was etched on one of the glass cell boundaries. The polarizers were oriented at 45° with the planar anchoring direction x. The thicker region was more birefringent and appeared brighter between crossed polarizers than the thinner region. N is the untextured nematic phase, L is a texture with stripes approximately parallel to x, whereas stripes of the sL texture show a transverse striation. The S-texture is a honeycomb-like assembly of focal conic domains (FCDs) characteristic of the smectic phase.

Fig. 2 shows the textures formed across a step in a region with large thickness, $h \geq 2.0$ μm, as the temperature was decreased from the N phase. At high temperatures, the N phase did not show any texture and appeared completely dark between crossed polarizers when the planar anchoring direction x was set parallel or perpendicular to the polarizers, showing that **n** was indeed distorted in the xz plane with $n_y = 0$. When x was at 45° with the crossed polarizers, the optical transmission slightly decreased as the temperature was decreased toward the S phase. This shows that **n** rotated slightly toward the surface normal but remained distorted, in contrast with the theoretical prediction that **n** should become uniform (36) due to the divergence of the bend elastic constant K_3 approaching the N-to-S transition (27, 37, 38). Instead, longitudinal stripes appeared approximately parallel to the anchoring direction x (L-texture) and acquired a transverse striation (sL-texture) as the temperature was decreased (Fig. 2). This texture continuously evolved into strings of fan-shaped focal conic domains (FCDs) as the temperature was further decreased and eventually into a close-packed "honeycomb" FCD pattern (S-texture, Fig. 2). Such texture is a hallmark of the S phase confined under hybrid anchoring conditions (2–5, 8, 24, 25, 39). Indeed, the constitutive feature of a FCD is that curved smectic layers keep a constant interlayer spacing or, equivalently, $\nabla\times\mathbf{n} = 0$. The centers of curvature of the layers describe two singular lines, a hyperbola and a confocal ellipse (1). Polarized fluorescent confocal microscopy revealed that the FCDs were of the

PROOF NOT FINAL EMBARGOED

"square" type already observed in 8CB films under nondegenerate hybrid anchoring conditions, i.e., with the ellipse at 45° from both the substrate and the asymptotes of the hyperbola (*SI Appendix*, Fig. S1) (8). Notably, the *S*-texture expanded from thick to thin regions of the film as the temperature was decreased (Fig. 2).

In regions with small thickness, $h \leq 1.5$ μm, the transverse striation of the *L*-texture rapidly expanded as the temperature was decreased and completely replaced the *L*-texture with a highly regular array perpendicular to *x* (*P*-texture, Fig. 3 *C* and *D*, *Right* side). Again, the transition proceeded from large to small thickness as the temperature was decreased (*SI Appendix*, Fig. S2). Both the *S*- and *P*-texture persisted when the temperature was decreased several degrees below the undistorted bulk transition temperature T_0.

The *L*-texture could not be extinguished between crossed polarizers due to a modulation of the in-plane director components (n_x, n_y) along the *y*-direction (Fig. 4 *A*, *B*, *E*, and *F*). In contrast, the *P*-texture could be extinguished when the stripes were parallel or perpendicular to the polarizer (Fig. 4 *C*, *D*, *G*, and *H*), showing that **n** lay in the *xz* plane, with n_x and n_z periodically modulated along the *x*-direction, and $n_y = 0$.

For intermediate film thicknesses, $h = (1.5$ to $2.0)$ μm, two different texture sequences were observed. In most cases the *L*-texture was replaced by a *P*-texture punctuated by clusters of FCDs with a string-like arrangement or patches of *S*-texture (Fig. 4 *D* and *H*). Only in a few samples the *L*-texture evolved into a continuous *S*-texture (Fig. 3 *B* and *C*, *Left* side). In all cases, the *P*-texture and *S*-texture never transformed into each other as the temperature was changed.

Calling T_c the temperature at which the *L*-texture changed into the *P*-texture, different values $T_{c,1}$ and $T_{c,2}$ were measured in region with different film thickness, respectively h_1 and h_2 (*SI Appendix*, Fig. S2). The temperature T_c increased as h increased and followed the relation $(T_{c,2} - T_{c,1})/T_0 = (h_0/h_1)^\gamma - (h_0/h_2)^\gamma$, where $h_2 > h_1$, $h_0 = (0.60 \pm 0.03)$ nm was determined by fitting (Fig. 5) and $\gamma = 0.98$ is calculated below.

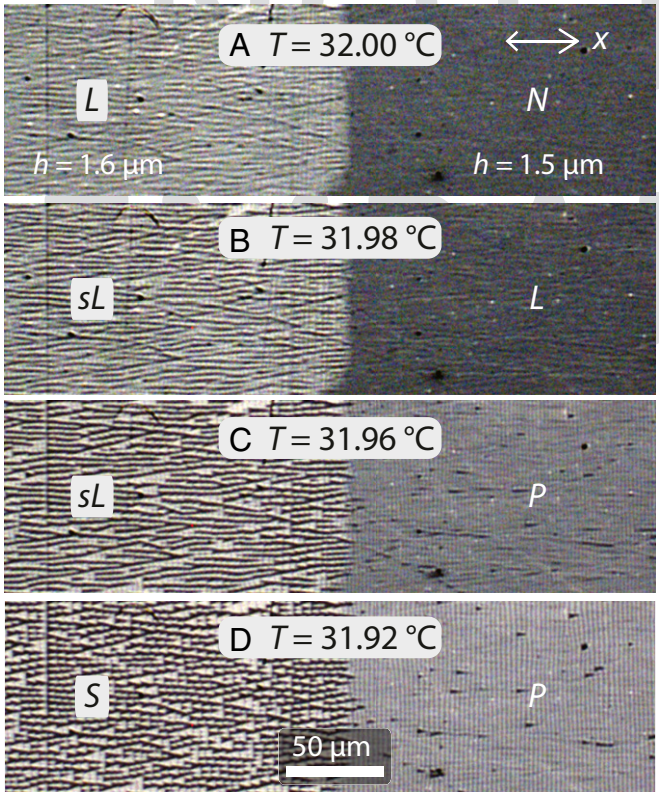


Fig. 3. Textures observed across a step of thickness upon cooling an 8CB film with intermediate (1.5 μm $< h < 2.0$ μm) and small ($h \leq 1.5$ μm) thickness. *P* is a texture with smooth and straight stripes perpendicular to the planar anchoring direction *x*.

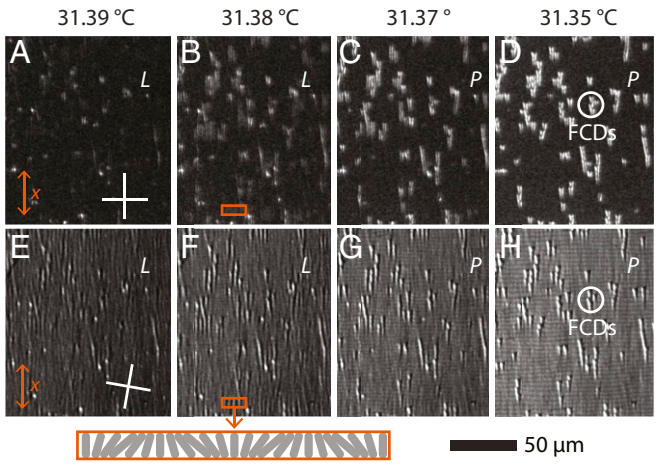


Fig. 4. Transition from the *L*-texture to the *P*-texture observed upon cooling an 8CB film with intermediate thickness (1.5 μm $< h < 2.0$ μm). The circles highlight an isolated cluster of FCDs within the *P*-texture. The cross indicates the direction of the crossed polarizers. (*A*–*D*) The *P*-texture was completely extinguished when the analyzer was parallel to the planar anchoring direction *x*, whereas the *L*-texture could not be extinguished. (*E*–*H*) The same region observed with the polarizers oblique to *x* to highlight the *P*-texture. The rectangle at the bottom schematically shows the in-plane director modulation of the *L*-texture.

When the temperature was decreased below T_c at one sample position with fixed h, the period d of the *P*-texture increased from the critical value $d_c = d(h, T_c)$ (Fig. 3 *C* and *D*, *Right*; Fig. 6*A*; and *SI Appendix*, Fig. S2 in SM). Near T_c, the slope of $(d - d_c)/d_c$ vs. temperature was 4.4 K^{-1} in average and did not correlate with d_c. The slope decreased and d became almost independent from temperature at room conditions, where previous observations were conducted (10, 20). When different thicknesses h (and therefore different temperatures T_c) were considered, the period d_c increased with h following an approximately linear relation: $d_c = d_0 + \alpha h$ with $d_0 = (0.6 \pm 0.1)$ μm and $\alpha = (1.1 \pm 0.1)$ (Fig. 6*B*). A linear dependence of d vs. h was previously observed also at room temperature, but with a larger slope $\alpha \sim 2$ (10, 20).

We also conducted a survey of pattern formation in smectic compounds differing from 8CB in molecular composition, properties, and phase sequences, using various aligning interfaces (e.g., solid/fluid, crystalline/amorphous, smooth/rough). The survey showed that *P*-texture invariably appears upon cooling the LC under nondegenerate hybrid anchoring conditions (*SI Appendix*, Figs. S3 and S4), clearly indicating that *P*-texture formation is a general phenomenon related to the *N*–*S* phase transition.

Discussion

To explain these results, we first note that the amplitude B of the bend distortion in the *N* phase is $B = |\nabla \times \mathbf{n}| \sim 1/h$ (27) and texture variations can be viewed as transition lines in a temperature-bend (T, B) phase diagram (Fig. 7*A*) analog to that of a superconductor (Fig. 1). The *S*-texture appears at low B and T values, when the *S* phase is fully established and the rotor field is expelled, analog to superconductor state of a metal. The observation that the *S*-texture grows from the *L*-texture upon cooling, expanding from thick to thin film regions (Fig. 2),

PROOF. NOT FOR PRINT

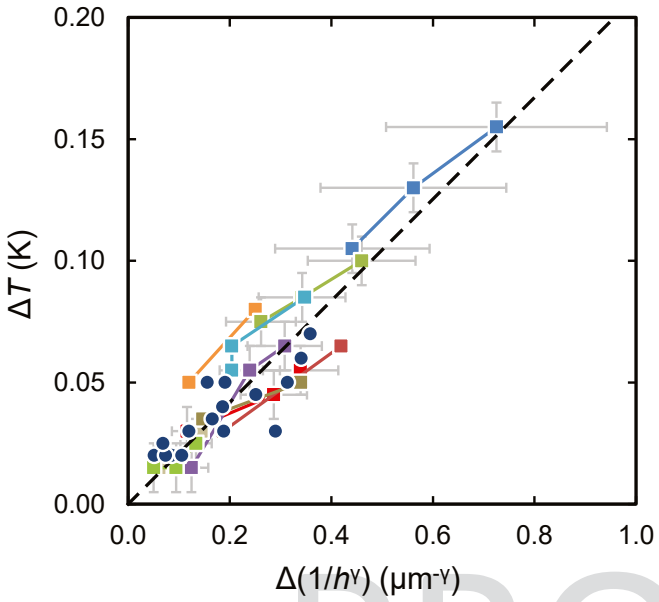


Fig. 5. Variation ΔT_c of the critical temperature for the appearance of the *P*-texture as a function of thickness variations $\Delta(1/h_\gamma)$. T_c was obtained upon cooling. The dotted line is a linear fit to the theoretical equation $\Delta T = T_0\Delta[(h_0/h)^\gamma]$ with $h_0 = (0.60 \pm 0.03)$ nm, $T_0 = 306.5$ K, and $\gamma = 0.98$. The circles and squares indicate measurements taken, respectively, across a step or at the crossing between two steps (each on opposite cell boundaries, *SI Appendix*, Fig. S2). Representative error bars are shown for three different measurements.

indicates that the transition line into the *S* phase has a negative slope $dB/dT < 0$ (Fig. 7). Since for $B = 0$ this transition occurs at the undistorted bulk transition temperature T_0, for $B > 0$ it must occur at a lower temperature. Therefore, the *L*-texture persists below T_0 and is either a depressed undercooled *N* phase or a frustrated smectic phase with penetration of the rotor field $\nabla\times\mathbf{n}$.

The latter possibility can be excluded based on the following arguments. Longitudinal stripes similar to the *L*-texture have been observed in LC films with hybrid anchoring conditions both near the *N*–*S* transition (24, 25, 39) and in the *N* phase of LCs that do not have a smectic phase (40). They can be theoretically explained for both degenerate and nondegenerate hybrid anchoring conditions as the result of an imbalance of elastic constants, leading to a mechanical instability with respect to small deviations of **n** from the *xz*-plane defined by the anchoring directions (25, 41–44). Longitudinal textures have also been observed under quasi-homeotropic (i.e., slightly hybrid) anchoring conditions (45) and occur in lieu of the Freedericksz's instability when the aligning field is perpendicular to a uniform director (22, 46, 47). In all cases, stripes appear in the *N* phase and approaching the *S* phase, if present. For 8CB, the bend K_3 and twist K_2 constants diverge at the *N*-to-*S* transition, while the splay constant K_1 stays finite: $K_3 >> K_2 >> K_1$ (38). The *L*-texture allows to partially exchange bend for twist and splay through a modulation of the director in the horizontal *xy*-plane, which cannot be extinguished between crossed polarizers (Fig. 4 *A*, *B*, *E*, and *F*). Importantly, stripe formation in the *N* phase can be explained without invoking any positional (smectic) order and can depress the *N* phase below T_0 (45). We therefore identify the *L*-texture as a modulated *N* phase that persists below T_0 with an incomplete relaxation of the bend distortion (i.e., incomplete expulsion of $\nabla\times\mathbf{n}$). The evolution of the *L*-texture into the *S*-texture has been studied for both degenerate

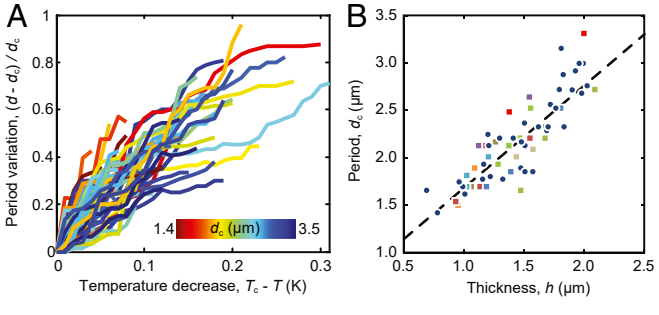


Fig. 6. Variation of the *P*-texture period *d* as a function of the temperature *T* and film thickness *h*. (*A*) Increase of *d* as a function of decreasing *T* relative to the critical values T_c and $d_c = d(T_c)$. Different colors indicate different values of d_c, specified in the color bar. (*B*) Increase of d_c with *h*. The dashed line has equation $d_c = d_0 + \alpha h$ with $d_0 = (0.6 \pm 0.1)$ μm and $\alpha = (1.1 \pm 0.1)$. The data and symbols correspond to those of Fig. 5.

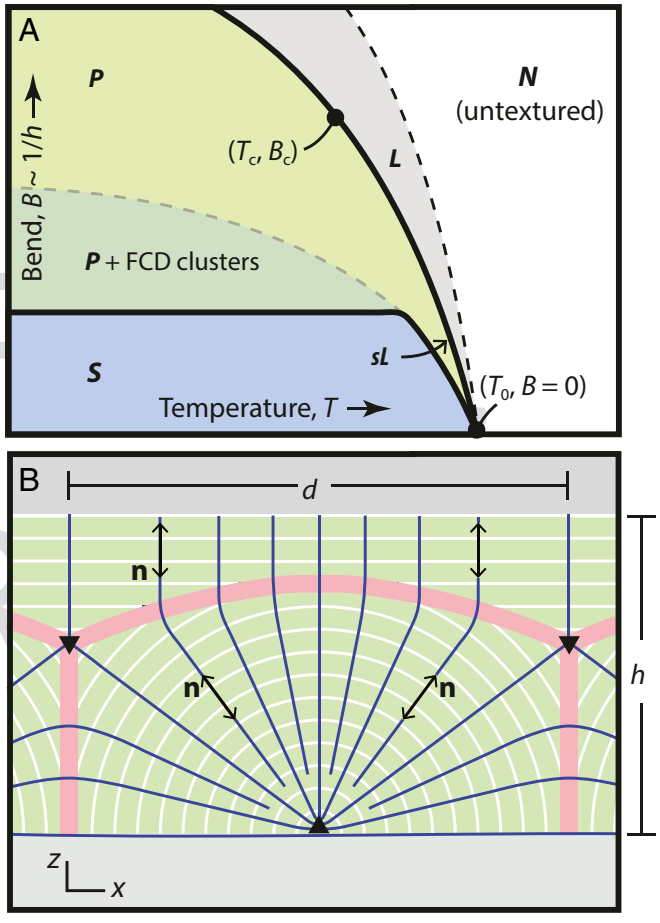


Fig. 7. (*A*) Schematic phase diagram of a type I smectic LC as a function of the temperature *T* and bend amplitude $B \sim 1/h$. The field *B*, untextured *N* phase, *S*-texture, and *P*-texture are analog to the magnetic field, normal state, superconductor state, and intermediate state of a type I superconductor, respectively (Fig. 1). The *L*-texture is a spontaneous director modulation of the undercooled *N* phase. (*B*) Internal structure of the *P*-texture. *x* and *z* are the directions of planar and homeotropic anchoring at the surfaces, respectively. The director **n** (blue lines) and smectic layers (white lines) in the bend-free regions are parallel and perpendicular to the *xz* plane, respectively. The bent undercooled *N* phase penetrates in the pink-shaded regions. The upward- and downward-pointing triangles indicate perpendicular disclinations lines with opposite strengths +1/2 and −1/2, respectively, ensuring zero charge of the overall director topology.

PROOF NOT FOR DISTRIBUTION

(25) or nondegenerate (24) hybrid anchoring conditions in the limit of small amplitudes B (i.e., large h).

Since the N phase, L-texture, and S-texture can be mapped into the normal metal, undercooled metal, and superconductor state, respectively, the analogy with superconductors suggests that the P-texture must be a frustrated smectic phase (Fig. 1). The type I or type II character of a rod-like thermotropic LC such as 8CB is determined by its molecular structure and intermolecular interactions (31). Common LC compounds optimized for electro-optics applications, including 9CB (33) and 8OCB (34), that are closely related to 8CB for molecular structure, order, and phase sequence, are known to be type I (1). Therefore, we identify P-texture formation in 8CB with the transition from the undercooled N phase to the intermediate phase of a type I LC. The analogy with type I superconductors is highlighted in Fig. 7*A* reproducing the typical features of the metal-superconductor phase diagram (Fig. 1). The intermediate state appears at temperatures T and amplitudes B immediately below a critical line with negative slope in the (T, B) phase diagram, and is eventually replaced by the S phase at low values of T and B, i.e., $\nabla\times\mathbf{n}$ is expelled (Fig. 7*A*) (28). The P-texture comprises periodically spaced S-phase domains (without bend) in equilibrium with regions of undercooled N phase (with bend) (Fig. 7*B*). Supporting the idea of a nematic-to-intermediate LC phase transition, first we note that evidence of a N phase persisting below T_0 in equilibrium with the S phase has emerged in studies of LCs subject to strong splay-bend (48, 49) or twist (35) distortions. Second, our survey of P-texture formation shows that it is a general phenomenon, independent from the choice of LC compound or substrates (*SI Appendix*, Figs. S3 and S4). Last, but most important, the critical temperature T_c of the transition from the undercooled N phase (L-texture) to the intermediate LC state (P-texture) decreases as the amplitude B increases (Fig. 5) in quantitative agreement with De Gennes' predictions, as shown below. In the N phase close to the S phase, the free energy density has the following form:

$$f = a|\psi|^2 + (b/2)|\psi|^4 + (C_{||}/2)\left|\nabla_{||}\psi - iq_0\mathbf{n}\right|^2 + (C_{\perp}/2)|\nabla_{\perp}\psi|^2 + (K_3/2)B^2 + (K_1/2)(\nabla\cdot\mathbf{n})^2, \quad [1]$$

where || and ⊥ indicate the direction parallel and perpendicular to $\mathbf{n}$, respectively (50). Eq. 1 is formally identical to the Ginzburg–Landau free energy functional of a superconductor, except for the last term. The director $\mathbf{n}$ plays the role of the magnetic vector potential, $\mathbf{B} = \nabla\times\mathbf{n}$ is equivalent to the magnetic field and q_0 to the charge $-2e$ of a Cooper electron pair. The first and second energy terms are required to create a uniform order parameter ψ, whereas the third and fourth term are required to create order gradients $\nabla\psi$ different from the ground-state gradient $iq_0\mathbf{n}$. The fifth term is the bend elastic energy of the LC that is analog to the magnetic energy in superconductors. The last term is specific to LCs and represents the splay elastic energy. Also, the coefficients $C_{||,\perp}$ of an LC are a priori different due to anisotropy. The key argument made by De Gennes in analogy with the normal-to-superconductor transition, is that the N-to-S transition occurs when the energy $(K_3/2)B^2$ equals the condensation energy $-a^2/2b$. Introducing the longitudinal coherence length $\xi = (C_{||}/2a)^{1/2}$ and bend penetration length $\lambda = (K_3b/C_{||}a)^{1/2}q_0$ (1, 27, 50), the equality can be written as $h = 1/B \sim 2^{1/2}q_0\xi\lambda$. In the N phase, $\xi = \xi_0 t^{-\nu}$, where $\xi_0 q_0 \sim 0.8$, $t = T/T_0 - 1$ is the reduced temperature and $\nu \sim 2/3$ is the critical exponent of the 3d-XY universality class (37, 51–53). The penetration length can also be written as $\lambda = (K_3/\beta)^{1/2}$, where $\beta = C_{||}(q_0|\psi_0|)^2$ is the layer compressibility modulus and ψ_0 is the undistorted bulk order parameter. K_3 diverges as ξ in the N phase (37, 38). Since the ratio of bare correlation lengths below (ξ_0^-) and above (ξ_0^+) the transition temperature T_0 is $\xi_0^-/\xi_0^+ = 3$ in a 3d-XY system the bend constant in the smectic phase is $K_3^- = 3K_3$ (34). On the other hand, the compressibility in the S phase shows a nonuniversal behavior: $\beta = \beta_0 + \beta_1|t|^{\phi}$ with $\beta_0 \sim 1\times10^6$ J/m^2 and $\beta_1 \sim 6\times10^6$ J/m^2, and an anomalous exponent $\phi \sim 0.47$ (54, 55). Using the values of K_3 and β from the literature (37, 38, 54, 55), the penetration length is found to be $\lambda = \lambda_0 t^{-\eta}$, where $\lambda_0 = 1.1$ nm and $\eta = 0.31$. The condensation condition $h \sim 2^{1/2}q_0\xi\lambda$ can therefore be written as $t_c = (h_0/h)^{\gamma}$, where $\gamma = \nu + \eta \sim 0.98$ and h_0 is a characteristic length. We also note that the Ginzburg parameter is $\kappa = \lambda^-/\xi^- = 3^{1/2}\lambda/3\xi = (1/3)^{1/2}(\lambda_0/\xi_0)t^{\nu-\eta} = 1.57t^{0.35} < 6\times10^{-2}$ over the entire temperature range of the smectic phase ($t < 4\times10^{-2}$). Therefore, the condition $\kappa < 1/2^{1/2}$ for type I character of 8CB is verified.

Fig. 5 shows that, indeed, the critical temperature T_c depends on the film thickness h in accord with the predicted dependence: $t_c = 1 - T_c/T_0 = (h_0/h)^{\gamma}$. A fit of the temperature differences $\Delta T_c = T_{c,2} - T_{c,1} = T_0 h_0^{\gamma}(1/h_1^{\gamma} - 1/h_2^{\gamma})$ provides the characteristic length $h_0 = 0.60$ nm, from which the bare penetration length $\lambda_0 = h_0/2^{1/2}q_0\xi_0 = 1.0$ nm can be calculated. This value is in remarkable agreement with the predicted value $\lambda_0 = 1.1$ nm and confirms that the L-to-P texture transition is indeed analog to the metal-to-intermediate state transition of type I superconductors.

The analogy also provides important insights into the (T, B) phase diagram of LCs. Transition lines become asymptotically parallel to the horizontal T-axis as temperature is decreased, so that the intermediate-to-superconductor and normal-to-intermediate transition lines intersect the vertical B axis, respectively, at values B_0 and B_1 in the limit $T \to 0$ (Fig. 1) (28). Therefore, either the metal-to-intermediate transition is observed as T is decreased with $B_1 > B > B_0$ or the metal stays in the undercooled normal state for $B > B_1$, without undergoing any transition. Indeed, only the transition from the undercooled nematic phase (i.e., L-texture) to the P-texture was observed in films thinner than $h_0 = 1.5$ μm, i.e., for bend amplitudes larger than $B_0 = 1/h_0$. The P-texture persisted for thicknesses as small as 0.6 μm (Fig. 6*B*) rather than being replaced by the untextured N phase, indicating that the limit field B_1 was not reached.

The analogy with superconductors (Fig. 1) also suggests that a P-to-S transition should occur for $B < B_0$. Therefore, the sequence $L \to P \to S$ should be observed as T is decreased at a fixed and sufficiently low value of B (Fig. 7*A*). This suggests that the *sL*-texture (Figs. 2 and 3 *B* and *C*), *Left* side) is an incomplete P-texture growing within the L-texture, whereas isolated FCD clusters (Fig. 4 *D* and *H*) are due to the incomplete growth of the S-texture within the P-texture. Nevertheless, the P-to-S transition was not clearly resolved in our experiments. A possible explanation is that the P-to-S transition line is almost horizontal for temperatures reaching values close to T_0, in analogy with thin metal films with a high depolarization factor (28). Therefore, either the P-texture or S-texture is created when B is above or below the horizontal line, respectively. Alternatively, the growth of the S-texture from the P-texture could be hindered by large energy barriers, i.e., the P-texture could persist as a metastable state below the "ghost" P-to-S transition line. It has been shown that applying an electric field while cooling from the N phase induces P-texture formation in thick 8CB, instead of the S-texture expected in the absence of fields (10). When the field is switched off, the P-texture persists as a metastable state at temperatures and thicknesses where the S-texture should be observed. This behavior is due to different arrays of topological defects in the P-texture and S-texture that cannot be transformed into each other without breaking strong topological constraints. Therefore, topological defects can effectively prevent the development of the S-texture from the P-texture as temperature is decreased.

PROOF NOT FINAL EMBARGOED

Predicting the formation or geometry of patterns in the intermediate state of superconductors is known to be a theoretical challenge that cannot be solved solely by minimizing the Ginzburg–Landau free energy (first five terms in Eq. 1) (29, 30). Theoretical modeling of the *P*-texture in LCs is further complicated by the additional splay energy term in Eq. 1 (1) and is beyond the scope of this article. However, the formation of 1d patterns at the transition into the intermediate state of both LC and superconductor films suggests a deep and general connection between frustration of the low-temperature (smectic or superconductor) phase and spontaneous breaking of symmetry in the film plane. It is noteworthy that the period d of the *P*-texture increases when T and/or B decrease in 8CB (Figs. 5 and 6), whereas the opposite behavior (pattern coarsening) is observed in the intermediate state of a metal (28–30). This suggests that d increases to accommodate periodically spaced domains of the *S* phase that grow to the expense of undercooled nematic regions. Fig. 7*B* shows the likely internal structure of the *P*-texture based on available experimental data (6, 9, 10, 23, 49, 56, 57). To satisfy both surface anchoring conditions and keep a constant layer spacing, the smectic layers tend to be flat and parallel near the surface inducing homeotropic anchoring, whereas they tend to form hemicylindrical domains near the surface inducing planar anchoring. Although previous models have tried to resolve the complex balance of bulk elastic forces and surface anchoring in the *P*-texture mainly by introducing various types of topological defects at the boundary between, the structure should also comprise domains of bent undercooled *N* phase at the boundary between curved but bend-free smectic domains. Further theoretical effort is needed to build a predictive model starting from Eq. 1.

Conclusions

Our study shows that fundamental aspects of the *N*–*S* phase transition can be studied by deforming the director field in thin LC films using external aligning field (i.e., surface interactions) (33–35), as opposed to observing thermodynamic fluctuations in uniform LC samples (37, 51–53). In particular, our findings confirm De Gennes' prediction of a depressed *N*-to-*S* transition leading to the "intermediate" frustrated smectic phase. In view of the bottom-up production of micropatterns with a large response to external stimuli, we anticipate that the 1d *P*-texture of the intermediate LC state can be conveniently produced by applying a strong electric field to a uniform LC film with planar anchoring conditions (10). Our findings are particularly relevant to the design of self-assembled LC templates that are used for guiding the ordering and assembly of functional nanoparticles into anisotropic structures with interesting plasmonic and charge-transport properties (9, 18–21).

Materials and Methods

The LC compound 8CB was purchased from Sigma-Aldrich. Homeotropic anchoring was obtained by dip-coating a glass substrate with a silane monolayer (octadecyl-trimethoxy-silane from Sigma-Aldrich), whereas unidirectional parallel anchoring was obtained by spin-coating the glass substrate with a thin polymer film (poly-imide PI2555 from Hitachi Chemical DuPont MicroSystems) that was gently rubbed with a velvet cloth along the anchoring direction.

Before depositing the silane and polymer, the surfaces were etched with a solution containing hydrofluoric acid to create channels with rectangular cross-sections, step-like edges narrower than 50 μm, and depths between 70 and 700 nm (58). The step height Δh was measured using a stylus profilometer (Dektak 8 by Veeco) with a precision of about 20 nm. After assembling the surfaces and before filling the cell with the LC, the thickness h was determined with an accuracy of about 20% via analysis of the cell's optical transmittance, showing multiple-beam interference due to reflections at air–glass interfaces.

The dependence of transition temperatures on the LC film thickness h (e.g., the difference ΔT in Fig. 5) was studied in a narrow region across a step-like edge to avoid temperature gradients, i.e., both sides of the step were at the same temperature. The cells were sealed in a temperature-controlled enclosure with 0.01 °C accuracy and observed in transmission between crossed polarizers. Note that the reported temperature values were read from the temperature controller and may differ from the actual values reached in the region where texture transitions were observed.

The authors have shared as *SI Appendix* all datasets appearing in this article.

ACKNOWLEDGMENTS. We are grateful to Charles Rosenblatt at Case Western Reserve University for his comments and suggestions. We thank Roberto Termine of Consiglio Nazionale delle Ricerche, Istituto di Nanotecnologia, for his help with the stylus profilometer. A.E.M. also acknowledges the support of the Scientific and Technical Research Council of Turkey–International Doctoral Research Fellowship Programme 2214/A.

1. P. Oswald, P. Pieranski, *Smectic and Columnar Liquid Crystals* (Taylor and Francis, 2006).
2. G. Friedel. Les états mésomorphes de la matière. *Ann. Phys. (Paris)* **18**, 273–474 (1922).
3. J. B. Fournier, I. Dozov, G. Durand, Surface frustration and texture instability in smectic-A liquid crystals. *Phys. Rev. A* **41**, 2252–2255 (1990).
4. L. Z. Ruan, J. R. Sambles, I. W. Stewart, Self-organized periodic photonic structure in a nonchiral liquid crystal. *Phys. Rev. Lett.* **91**, 033901 (2003).
5. M. C. Choi *et al.*, Ordered patterns of liquid crystal toroidal defects by microchannel confinement. *Proc. Natl. Acad. Sci. U.S.A.* **101**, 17340–17344 (2004).
6. J. P. Michel *et al.*, Optical gratings formed in thin smectic films frustrated on a single crystalline substrate. *Phys. Rev. E Stat. Nonlin. Soft Matter Phys.* **70**, 011709 (2004).
7. B. Zappone, E. Lacaze, Surface-frustrated periodic textures of smectic-A liquid crystals on crystalline surfaces. *Phys. Rev. E Stat. Nonlin. Soft Matter Phys.* **78**, 061704 (2008).
8. B. Zappone, C. Meyer, L. Bruno, E. Lacaze, Periodic lattices of frustrated focal conic defect domains in smectic liquid crystal films. *Soft Matter* **8**, 4318–4326 (2012).
9. D. Coursault *et al.*, Linear self-assembly of nanoparticles within liquid crystal defect arrays. *Adv. Mater.* **24**, 1461–1465 (2012).
10. I. Gryn, E. Lacaze, R. Bartolino, B. Zappone, Controlling the self-assembly of periodic defect patterns in smectic liquid crystal films with electric fields. *Adv. Funct. Mater.* **25**, 142–149 (2015).
11. Y. H. Kim *et al.*, Optically selective microlens photomasks using self-assembled smectic liquid crystal defect arrays. *Adv. Mater.* **22**, 2416–2420 (2010).
12. B. Son *et al.*, Optical vortex arrays from smectic liquid crystals. *Opt. Express* **22**, 4699–4704 (2014).
13. F. Serra *et al.*, Curvature-driven, one-step assembly of reconfigurable smectic liquid crystal "compound eye" lenses. *Adv. Opt. Mater.* **3**, 1287–1292 (2015).
14. D. K. Yoon *et al.*, Internal structure visualization and lithographic use of periodic toroidal holes in liquid crystals. *Nat. Mater.* **6**, 866–870 (2007).
15. Y. H. Kim *et al.*, Fabrication of a superhydrophobic surface from a smectic liquid-crystal defect array. *Adv. Funct. Mater.* **19**, 3008–3013 (2009).
16. Y. H. Kim, D. K. Yoon, H. S. Jeong, H. T. Jung, Self-assembled periodic liquid crystal defects array for soft lithographic template. *Soft Matter* **6**, 1426–1431 (2010).
17. Y. H. Kim, D. K. Yoon, H. S. Jeong, O. D. Lavrentovich, H. T. Jung, Smectic liquid crystal defects for self-assembling of building blocks and their lithographic applications. *Adv. Funct. Mater.* **21**, 610–627 (2011).
18. D. Coursault *et al.*, Tailoring anisotropic interactions between soft nanospheres using dense arrays of smectic liquid crystal edge dislocations. *ACS Nano* **9**, 11678–11689 (2015).
19. A. Honglawan *et al.*, Synergistic assembly of nanoparticles in smectic liquid crystals. *Soft Matter* **11**, 7367–7375 (2015).
20. I. Gryn, E. Lacaze, L. Carbone, M. Giocondo, B. Zappone, Electric-field-controlled alignment of rod-shaped fluorescent nanocrystals in smectic liquid crystal defect arrays. *Adv. Funct. Mater.* **26**, 7122–7131 (2016).
21. B. Rožič *et al.*, Oriented gold nanorods and gold nanorod chains within smectic liquid crystal topological defects. *ACS Nano* **11**, 6728–6738 (2017).
22. M. Goscianski, L. Leger, A. Mircea-Roussel, Field induced transitions in smectic A phases. *J. Phys. Lett.* **36**, 313–316 (1975).
23. O. Parodi, A possible magnetic transition in smectics-A. *Solid State Commun.* **11**, 1503–1507 (1972).
24. P. E. Cladis, S. Torza, Growth of a smectic A from a bent nematic phase and the smectic light valve. *J. Appl. Phys.* **46**, 584–599 (1975).
25. M. J. Gim, D. A. Beller, D. K. Yoon, Morphogenesis of liquid crystal topological defects during the nematic-smectic A phase transition. *Nat. Commun.* **8**, 15453 (2017).
26. A. Yethiraj, "Recent experimental developments at the nematic to smectic-A liquid crystal phase transition" in *Thermotropic Liquid Crystals: Recent Advances*, A. Ramamoorthy, Ed. (Springer, 2007), pp. 235–248.
27. P. G. De Gennes, An analogy between superconductors and smectics A. *Solid State Commun.* **10**, 753–756 (1972).
28. C. P. Poole, H. A. Farach, R. J. Creswik, R. Prozorov, *Superconductivity* (Academic Press, London, UK, 2007).

PROOF
NOT FINAL
EMBARGOED

29. R. Prozorov, Equilibrium topology of the intermediate state in type-I superconductors of different shapes. *Phys. Rev. Lett.* **98**, 257001 (2007).
30. R. Prozorov, A. F. Fidler, J. R. Hoberg, P. C. Canfield, Suprafroth in type-I superconductors. *Nat. Phys.* **4**, 327–332 (2008).
31. S. R. Renn, T. C. Lubensky, Abrikosov dislocation lattice in a model of the cholesteric-to-smectic-A transition. *Phys. Rev. A Gen. Phys.* **38**, 2132–2147 (1988).
32. H. T. Nguyen *et al*. TGB_A and TGB_C phases in some chiral tolan derivatives. *J. Phys. II France* **2**, 1889–1906 (1992). Q:12
33. I. Dozov, G. Durand, Quantized grain boundaries in bent smectic-A liquid crystals. *Eur. Phys. Lett.* **28**, 25–30 (1994).
34. R. Wang, I. M. Syed, G. Carbone, R. G. Petschek, C. Rosenblatt, Bend-induced melting of the smectic-A phase: Analogy to a type-I superconductor. *Phys. Rev. Lett.* **97**, 167802 (2006).
35. L. Z. Ruan, M. A. Osipov, J. R. Sambles, Coexisting nematic and smectic-A phases in a twisted liquid-crystal cell. *Phys. Rev. Lett.* **86**, 4548–4551 (2001).
36. G. Barbero, R. Barberi, Critical thickness of a hybrid aligned nematic liquid crystal cell. *J. Phys.* **44**, 609–616 (1983).
37. D. Davidov *et al*., High-resolution x-ray and light-scattering study of critical behaviour associated with the nematic-smectic-A transition in 4-cyano-4′-octylbiphenyl. *Phys. Rev. B Condens. Matter* **19**, 1657–1663 (1979).
38. M. J. Bradshaw, E. P. Raynes, J. D. Bunning, T. E. Faber, The Frank constants of some nematic liquid-crystals. *J. Phys.* **46**, 1513–1520 (1985).
39. H. L. Liang, R. Zentel, P. Rudquist, J. Lagerwall, Towards tunable defect arrangements in smectic liquid crystal shells utilizing the nematic-smectic transition in hybrid-aligned geometries. *Soft Matter* **8**, 5443–5450 (2012).
40. O. D. Lavrentovich, V. M. Pergamenshchik, Stripe domain phase of a thin nematic film and the K13 divergence term. *Phys. Rev. Lett.* **73**, 979–982 (1994).
41. A. Sparavigna, L. Komitov, O. D. Lavrentovich, A. Strigazzi, Saddle-splay and periodic instability in a hybrid aligned nematic layer subjected to a normal magnetic-field. *J. Phys. II* **2**, 1881–1888 (1992).
42. V. M. Pergamenshchik, Surfacelike-elasticity-induced spontaneous twist deformations and long-wavelength stripe domains in a hybrid nematic layer. *Phys. Rev. E Stat. Phys. Plasmas Fluids Relat. Interdiscip. Topics* **47**, 1881–1892 (1993).
43. A. Sparavigna, O. D. Lavrentovich, A. Strigazzi, Periodic stripe domains and hybrid-alignment regime in nematic liquid crystals: Threshold analysis. *Phys. Rev. E Stat. Phys. Plasmas Fluids Relat. Interdiscip. Topics* **49**, 1344–1352 (1994).
44. O. V. Manyuhina, M. Ben Amar, Thin nematic films: Anchoring effects and stripe instability revisited. *Phys. Rev. A* **377**, 1003–1011 (2013).
45. V. M. Pergamenshchik, I. Lelidis, V. A. Uzunova, Stripe domains in a nearly homeotropic nematic liquid crystal: A bend escaped state at a nematic-smectic-A transition. *Phys. Rev. E Stat. Nonlin. Soft Matter Phys.* **77**, 041703 (2008).
46. C. Gooden *et al*., Simultaneous magnetic-deformation and light-scattering study of bend and twist elastic-constant divergence at the nematic-smectic-A phase transition. *Phys. Rev. Lett.* **54**, 1035–1038 (1985).
47. F. Lonberg, R. B. Meyer, New ground state for the Splay-Fréedericksz transition in a polymer nematic liquid crystal. *Phys. Rev. Lett.* **55**, 718–721 (1985).
48. J.-P. Michel *et al*., Structure of smectic defect cores: X-ray study of 8CB liquid crystal ultrathin films. *Phys. Rev. Lett.* **96**, 027803 (2006).
49. D. Coursault *et al*., Self-organized arrays of dislocations in thin smectic liquid crystal films. *Soft Matter* **12**, 678–688 (2016).
50. P. G. De Gennes, J. Prost, *The Physics of Liquid Crystals* (Oxford University Press, Oxford, UK, ed. 2, 1993).
51. J. D. Litster *et al*., High resolution x-ray and light scattering studies of bilayer smectic A compounds. *J. Phys. Colloq.* **40**, 339–340 (1979).
52. S. Sprunt, L. Solomon, J. D. Litster, Equality of X-ray and light scattering measurements of coherence lengths at the nematic-smectic-a phase transition. *Phys. Rev. Lett.* **53**, 1923–1926 (1984).
53. A. Primak, M. Fisch, S. Kumar, Critical behavior at the nematic-to-smectic-A transition in a strong magnetic field. *Phys. Rev. Lett.* **88**, 035701 (2002).
54. M. Fisch, P. S. Pershan, L. B. Sorensen, Absolute measurement of the critical behavior of the smectic elastic constant of bilayer and monolayer smectic-A liquid crystals on approaching the transition to the nematic phase. *Phys. Rev. A* **29**, 2741–2750 (1984).
55. M. Benzekri, T. Claverie, J. P. Marcerou, J. C. Rouillon, Nonvanishing of the layer compressional elastic constant at the smectic-A-to-nematic phase transition: A consequence of Landau-Peierls instability? *Phys. Rev. Lett.* **68**, 2480–2483 (1992).
56. B. Zappone *et al*., Self-ordered arrays of linear defects and virtual singularities in thin smectic-A films. *Soft Matter* **7**, 1161–1167 (2011).
57. D. Coursault *et al*., Modeling the optical properties of self-organized arrays of liquid crystal defects. *Opt. Express* **22**, 23182–23191 (2014).
58. A. Zacheo *et al*., Fast and safe microwave-assisted glass channel-shaped microstructure fabrication. *Lab Chip* **15**, 2395–2399 (2015).

PROOF
NOT FINAL
EMBARGOED

AUTHOR QUERIES

AUTHOR PLEASE ANSWER ALL QUERIES

Q: 1_Please review 1) the author affiliation and footnote symbols, 2) the order of the author names, and 3) the spelling of all author names, initials, and affiliations and confirm that they are correct as set.

Q: 2_Please review the information in the author contribution footnote carefully. Please make sure that the information is correct and that the correct author initials are listed. Note that the order of author initials matches the order of the author line per journal style. You may add contributions to the list in the footnote; however, funding should not be an author's only contribution to the work.

Q: 3_Please review your open access and license selection and confirm that it is correct.

Q: 4_Certain compound terms are hyphenated when used as adjectives and unhyphenated when used as nouns. This style has been applied consistently throughout where (and if) applicable.

Q: 5_If you have any changes to your Supporting Information (SI) file(s), please provide revised, ready-to-publish replacement files without annotations.

Q: 6_In sentence beginning "Our findings provide. . .." (in the abstract): Claims of priority or primacy are not allowed, per PNAS policy (https://www.pnas.org/page/authors/format); therefore, the term "new" has been deleted.

Q: 7_For affiliations line: Please confirm that "Università del Salento" is the correct institution for affiliation *d*.

Q: 8_Please check all math, equations, and variables in the text for accuracy in typesetting, including typeface (roman or italic), letters, numbers, and symbols to ensure they are complete and displaying properly.

Q: 9_For ref. 2: This reference has been updated. Please confirm title of article and page range.

Q: 10_For ref. 8: This reference has been updated. Please confirm last page number.

Q: 11_For ref. 26: This reference has been updated. Please confirm page range of chapter.

Q: 12_For ref. 32: This reference has been updated. Please confirm article title.

Q: 13_For Fig. 2 legend: Please cite panels *A–D* in the figure legend.

Q: 14_For Fig. 3 legend: Please cite panels *A–D* in the figure legend.